

AperTO - Archivio Istituzionale Open Access dell'Università di Torino

## Integration, qualification, and launch of the Mini-EUSO telescope on board the ISS

**This is a pre print version of the following article:**

*Original Citation:*

*Availability:*

This version is available <http://hdl.handle.net/2318/1946722> since 2023-12-08T09:36:05Z

*Published version:*

DOI:10.1007/s12210-023-01142-8

*Terms of use:*

Open Access

Anyone can freely access the full text of works made available as "Open Access". Works made available under a Creative Commons license can be used according to the terms and conditions of said license. Use of all other works requires consent of the right holder (author or publisher) if not exempted from copyright protection by the applicable law.

(Article begins on next page)

# Integration, qualification and launch of the Mini-EUSO telescope on board the ISS

Laura Marcelli<sup>1\*</sup> and autori articolo UV<sup>2</sup>

<sup>1\*</sup>INFN, Section of Rome Tor Vergata, Via della Ricerca Scientifica 1, Rome, I-00173, Italy.

<sup>2</sup>Department, Organization, Street, City, 10587, State, Country.

\*Corresponding author(s). E-mail(s):

[laura.marcelli@roma2.infn.it](mailto:laura.marcelli@roma2.infn.it);

Contributing authors: [iiauthor@gmail.com](mailto:iiauthor@gmail.com);

## Abstract

Mini-EUSO is a high sensitivity imaging telescope that observes the Earth from the ISS in the near ultraviolet band (290÷430 nm), through the nadir-facing, UV-transparent window in the Russian Zvezda module. The instrument, launched in 2019, has a field of view of 44°, a spatial resolution on the Earth surface of 6.3 km and a temporal sampling rate of 2.5 microseconds. Thanks to its triggering and on-board processing, the telescope is capable of detecting UV emissions of cosmic, atmospheric and terrestrial origin on different time scales, from a few microseconds upwards. The optics is composed of two Fresnel lenses focusing light onto an array of 36 Hamamatsu multi-anode photomultiplier tubes, for a total of 2304 pixels. The telescope also contains two cameras in the near infrared and visible, an 8 by 8 array of Silicon-PhotoMultipliers and a series of UV sensors to manage night-day transitions. The scientific objectives range from atmospheric phenomena (Lightning, Transient Luminous Events, ELVES), study of meteoroids, search of interstellar meteoroids and strange quark matter, mapping of the Earth's nocturnal emissions in the ultraviolet range, search of cosmic rays with energy above 10<sup>21</sup> eV. The instrument has been integrated and qualified in 2019, with final tests in Baikonur prior to its launch. Operations involve periodic installation in the Zvezda module and observations at night time, with periodic downlink of data samples, with the full data being sent to the ground via pouches containing the data discs. Mission planning involves the selection of the optimal orbits to maximize the science return of the instrument. In this work we will describe

the various phases of construction, testing and qualification prior to the launch and in-flight operations of the instrument on board the ISS.

**Keywords:** UV telescope, UV emissions, ISS, meteors, SQM, Transient Luminous Events, UHECRs.

## 1 Introduction

Mini-EUSO (Multiwavelength Imaging New Instrument for the Extreme Universe Space Observatory) experiment [1] is part of the JEM-EUSO program led by the JEM-EUSO (Joint Experiment Missions - Extreme Universe Space Observatory) Collaboration. This program aims to detect and study Ultra High Energy Cosmic Rays (UHECRs) from space for the first time. The space-based observation of UHECRs is complementary to that from ground-based observatories and allows to have a much wider observed area than with on-ground detectors and observe both of Earth's hemispheres with only one instrument, thus reducing the possible systematic uncertainty.

Over the years, the collaboration carried on various experiment operating on ground (EUSO-TA [2] (2013-)), on stratospheric balloons (EUSO-Balloon [3, 4] (2014), EUSO-SPB1 [5] (2017)) and in space (TUS [6] (2016)) and others are planned for the upcoming years: EUSO-SPB2 [7] on stratospheric balloon (launch foreseen in 2023) and two future space missions K-EUSO [8] and POEMMA [9, 10].

Mini-EUSO was launched to the ISS by the uncrewed Soyuz MS-14 on August 22, 2019, from the Bajkonur Cosmodrome (Kazakhstan). The first installation of the instrument on the UV-transparent window in the Zvezda module took place on October 7, when the first session of data taking was performed. Since then, it has been taking data periodically, with installations occurring every couple of weeks for a total of about 70 sessions over three years.

## 2 The telescope

The Mini-EUSO telescope [1] operates in the UV range (290 - 430 nm) from the nadir-facing UV transparent window in the Zvezda module of the International Space Station (ISS). The telescope has a square field of view of  $\simeq 44^\circ$ , a spatial resolution of  $\simeq 6.3 \text{ km}^2$  on Earth surface (depending on the ISS altitude) and it is capable of single photon counting detection.

Mini-EUSO optical system consists of two Fresnel lenses, with a diameter of 25 cm, focusing the light onto a focal surface, or Photon Detector Module (PDM), composed by an array of 6 x 6 Hamamatsu MultiAnode Photomultipliers (MAPMTs) tubes, 64 pixels each, for a total of 2304 pixels (see Figure 1, left-hand side). Each MAPMT is powered by a Cockroft-Walton power supply board and presents a BG3 UV bandpass filter on the entry window. The PDM front-end electronics consists of 6 SPACIROC3 (Spatial Photomultiplier Array

Counting Integrated ReadOutChip [11]) boards. Data are then processed by a Xilinx Zynq based FPGA board which implements a multi-level triggering [12, 13], allowing the measurement of triggered UV transients for 128 frames at time scales of both  $2.5 \mu\text{s}$  and  $320 \mu\text{s}$ . Moreover, an untriggered acquisition mode with 40.96 ms frames performs a continuous data taking. The instrument is also equipped with two ancillary cameras to complement the UV measurements in the near infrared and visible range [14], three single pixel UV sensors used to manage day/night transitions and with a  $8 \times 8$  SiPM imaging array [15].

Data collection and storage onto 512 GB USB Solid State Disk (SSD) cards, inserted in the side of the telescope by the astronauts, is managed by a PCIe/104 form factor CPU.

Coupling to the window is done via a mechanical adapter flange and the only connection to the ISS is via a 28 V power supply and grounding cable. The Mini-EUSO power consumption is about 60 W. The instrument dimensions are  $37 \times 37 \times 62 \text{ cm}^3$  and its weight is about 35 kg (including the 5 kg adapter flange). As all instruments operating in the ISS and managed by cosmonauts and astronauts, the Mini-EUSO design is consistent with the safety requirements (no sharp edges, low surface temperature, robustness...).

The instrument has been integrated at the INFN Laboratories of Frascati and Rome Tor Vergata. Figure 1 shows some pictures taken during the integration of the Flight Model (FM). See [1] for more details about the telescope description and its first observations.

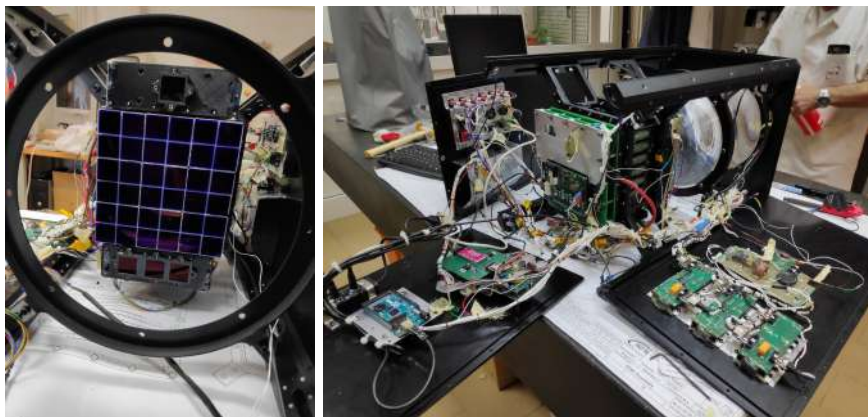


**Fig. 1** Mini-EUSO detector during the integration. **Left:** Mini-EUSO focal surface seen through the frame of the second lens. UV sensors are visible below the photomultiplier array, while the SiPM array is located above it. **Right:** all the mechanics, electronics and the two Fresnel lenses are clearly visible.

### 3 Space Qualification Tests

Two copies of the detector have been realized: the Engineering Model (EM) and the Flight Model (FM). The two models are identical except that in the EM only the four central MAPMTs are present and the other elements are replaced with mass dummies. Moreover in the EM the Fresnel lenses are replaced with flat PMMA elements with the same weight.

Both EM and FM underwent various qualification tests to ensure that they could withstand the transportation to the launch site, the launch and operations on the ISS. These included vibration and shock, ElectroMagnetic Interference and Compatibility (respectively EMI and EMC) and thermal-vacuum/environmental tests [16]. Vibrations tests had a more severe profile for the EM. After acceptance tests in Rome and Moscow, the EM is now being used as a training model for the various crews who operate it on the ISS.

#### 3.1 Random vibration and Shock Tests

The relatively high mass (35 kg) of the telescope required it to be launched in a hard-mounted (with bolts coupling it to the hull) configuration inside the Soyuz capsule. This translates in higher shock and random vibration loads on the hardware. Random vibration and shock tests took place at MATE srl premise (Torrita di Siena - Italy) in February (EM) and May (FM) 2019.

Tri-axial accelerometers for monitoring were placed on the detector and the vibrating plate as feedback and for reference. In Figure 2 the test setup with the Mini-EUSO telescope bolted on the vibration/shock plate.

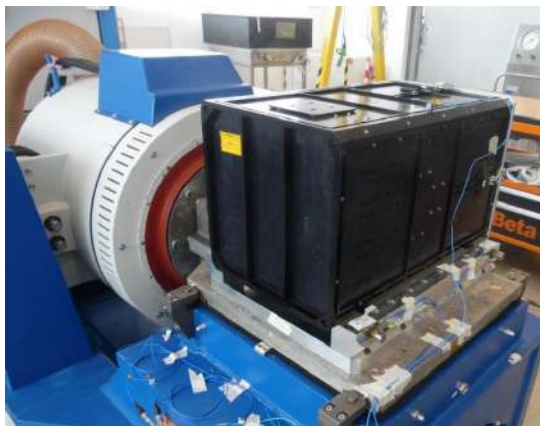


**Fig. 2** Mini-EUSO bolted on the vibration/shock plate.

The EM was subjected to random vibration tests with test sequence of 120, 480 and 600 seconds along the three axes in the frequency range from 20 to 2000 Hz to simulate the vibrations of the launch during the insertion (120 and 480 s sequences) and the vibrations during the orbital flight (600 s

sequence). Shock acceleration tests (up to  $\pm 40$  g) instead simulate the firing of the pyrotechnic shocks that separate the various rocket stages.

A summary of the performed tests on EM is reported in Table 1.

**Table 1** Random vibration and shock test specifications.

<b>A) Random vibration: axis X, Y and Z</b>
Resonance survey
Random vibration (insertion) - 120 ms with an overall strength of 7.42 g
Random vibration (insertion) - 480 ms with an overall strength of 3.58 g
Random vibration (orbital flight) - 600 ms with an overall strength of 3.84 g
Resonance survey to detect changes before/after vibration
<b>B) Shock along the axis X, Y and Z</b>
Resonance survey
Seven shock with 3 ms duration, $\pm 40$ g strength
Resonance survey to detect changes before/after shock

To detect if the vibrations or the shocks have resulted in internal damage, loosening of parts, or changes in the structure of the detector, a resonance survey was performed. This is done subjecting the telescope to a low vibration profile measuring the frequency response of the accelerometers located on the instrument before and after each test. Structural changes in the detector would be reflected in a change of the resonance frequencies.

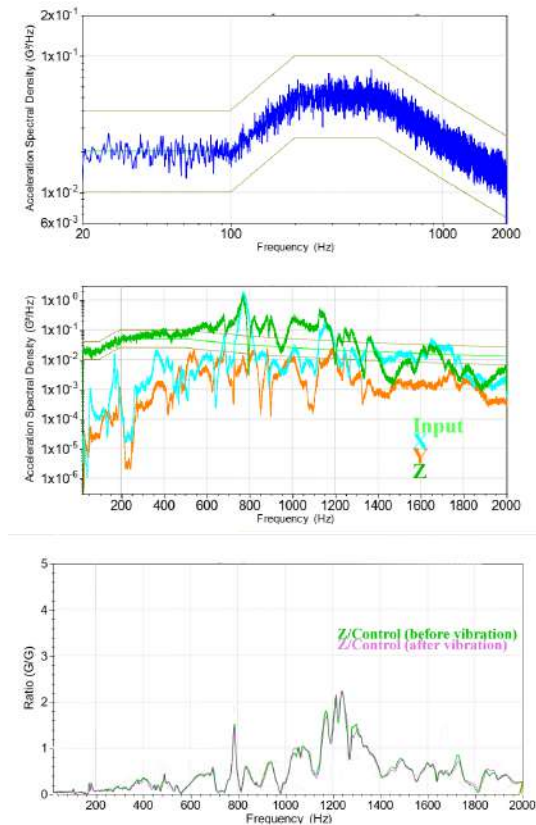
As an example, in Figures 3 and 4 are shown the Mini-EUSO EM responses after the random vibration along the Z-axis (duration 120 s, overall strength 7.42 g) and shock along positive X-axis direction respectively, together with the corresponding resonance shift survey.

### 3.2 EMI-EMC Tests

EMI-EMC tests are performed to verify that the Mini-EUSO instrument does not produce any undesired electromagnetic radiated emissions and that, conversely, it is capable to withstand external electromagnetic interference.

The EM has been subjected to emission and susceptibility tests in an anechoic chamber to verify its electromagnetic compatibility requirements. The tests performed are: Low and High Frequency (LF and HF) conductive interference, Low and High Frequency (LF and HF) conductive interference susceptibility, conducted pulse interference, electrical field intensity produced by High Frequency emissions. All these tests have been executed at the qualified GSD Laboratories in Pisa, Italy, during the month of January 2019 (see Table 2 for their specifications).

In the top of Figure 5 are shown two pictures of test set-up during the measurement of the electric field intensity produced by HF emissions when the detector is powered on at 28 V. In the same Figure, at the bottom, are shown

6 *Mini-EUSO telescope on board the ISS*

**Fig. 3** Mini-EUSO EM response after a random vibration (duration 120 s, overall strength 7.42 g) along the Z-axis. **Top panel:** Input Acceleration Spectral Density. The straight lines represent the acceptable range of vibration and the blue plot is the instantaneous reading by the accelerometer on the vibrating plate. **Centre panel:** Measured acceleration spectra on the three axes of Mini-EUSO. The brown and green straight lines show the input spectrum (the same of the Top Panel). Note how the structure of the instrument is such that the acceleration can exceed the input spectrum by about a factor 100 around 750 Hz. This does not pose any problem, since the frequency is high enough that no damage is induced to the instrument. **Bottom Panel:** the resonance shift survey along the Z-Axis. This compares the two resonance spectra (green: before vibration, purple: after vibration) to ensure that there are no changes - and most important no frequency shifts that would denote damage to the structure - after the vibration.

the antenna frequency profile responses, respectively, when the antenna is vertically (left) and horizontally (right) located near the detector. Mini-EUSO must not generate interference levels greater than the thresholds specified in Figure (red line) when powered at the range of supply voltages (between 23 and 29, with nominal 28 V). During the tests the detector was located in an anechoic chamber in vertical position analogous to the data-taking configuration on board the ISS, with the front end of the telescope (the one with the entrance lens) faces the ground plane.

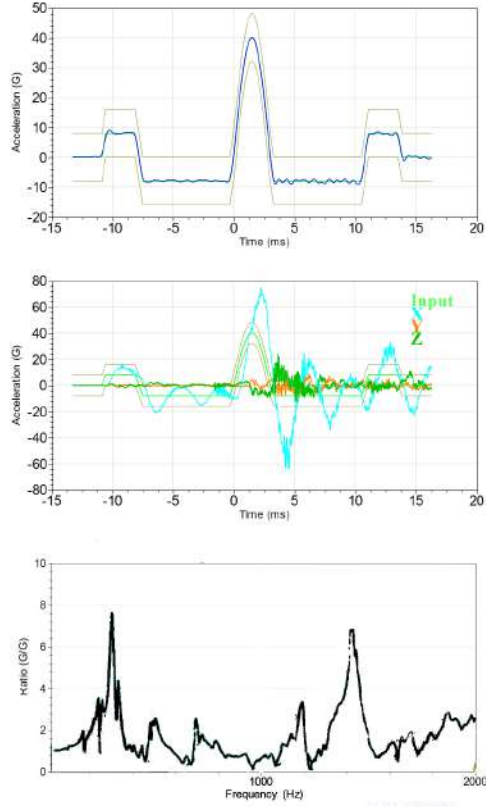


**Fig. 4** Mini-EUSO EM response after shock test session along the positive X-axis direction. **Top panel:** Input Acceleration as function of time. The straight lines represent the acceptable range of vibration and the blue plot is the instantaneous reading by the accelerometer on the vibrating plate. **Centre panel:** Measured acceleration spectra on the three axes of Mini-EUSO. The brown and green straight lines show the input spectrum (the same of the Top Panel). The acceleration profiles as a function of time for the three axes are also shown. Note how the vibration on the X-axis (the same of the shock) exceeds the input value of the the control channel (top) and of the instrument (bottom, azure: X-axis, orange: Y-axis, green: Z-axis). **Bottom Panel:** the resonance shift survey after shock test along X-axis. The two curves (before and after) are indistinguishable, a sign that there were no changes in the structure of the detector.

**Table 2** EMI/EMC tests specifications.

EMI/EMC	Frequency range (MHz)
Low-Frequency conductive interference	$(0.03 \div 10) * 10^{-3}$
High-Frequency conductive interference	0.01 $\div$ 100
Low-Frequency conductive interference susceptibility	$(0.02 \div 10) * 10^{-3}$
High-Frequency conductive interference susceptibility	0.01 $\div$ 300
Electrical field intensity produced by HF emissions	0.01 $\div$ 1000

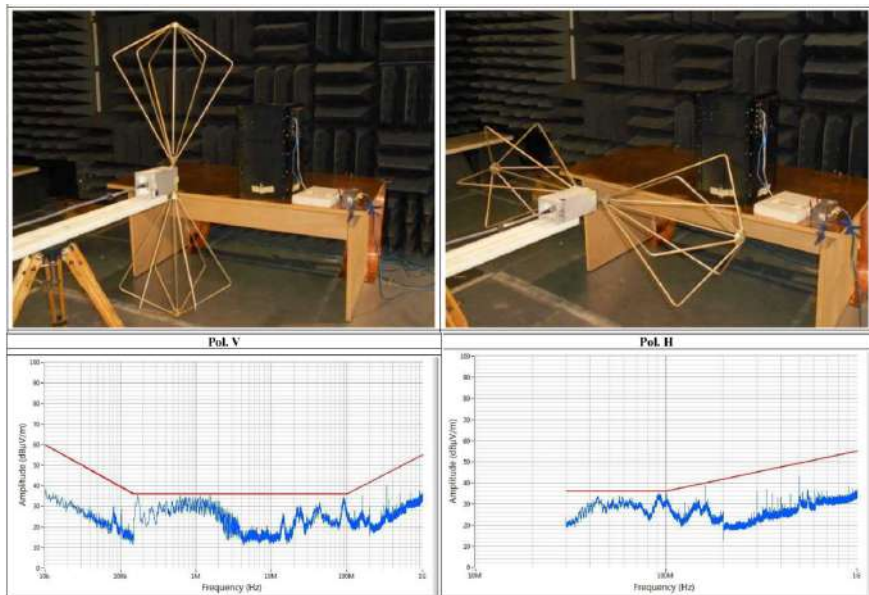


**Fig. 5 Top:** Test set-up during the measurement of the electric field intensity produced by HF emissions when the detector is powered on at 28 V and the antenna (left in the pictures) is vertically (left panel) and horizontally (right panel) located near the detector (right in the picture, placed on a copper plate acting as ground). **Bottom:** The measured emissions as a function of frequency (blue) compared with the maximum acceptable level (red curves) for a vertical (left) and horizontal (right) oriented antenna.

Moreover a start-up and in-rush current test was performed to assure that the start-up currents flowing into the device didn't exceed the maximum steady-state operating current and its rise and fall complied other requirements.

### 3.3 Environmental Tests

The telescope underwent also various environmental (temperature, humidity, pressure) tests to verify it was capable to withstand the transportation, storage and launch conditions. It is worth noting that most of the extreme temperature and humidity tests can be experienced during transportation and storage in Baikonur, where temperature can drop below 40 degrees Celsius during winter and above 50 degrees Celsius during summer.

Thee conditions which might be experienced during the cargo transportation to the launch site and within the Soyuz capsule have been reproduced in a thermal chamber. During transportation to the Baikonur launch site, temperature excursions can range between  $\pm 50$  °C, depending on the time of the year, while the humidity can reach a level up to 90%. In the Soyuz, pressurized atmospheric conditions (450 to 970 mm Hg) are maintained during launch.

Several thermal cycles inside a thermal chamber were made at low and high temperatures,  $\pm 55$  °C, and with humidity levels up to 95%. Low (450 mm Hg)

and high (970 mm Hg) pressure tests have been also performed. After each test the instrument was switched on for a functional run.

## 4 Field tests

In June 2019, the instrument (FM) was also field-tested in the Apennine Mountains, close to the town of Paganico Sabino (Lat. 42°09'38''N, Long. 13°00'33''E), in Rome, from the roof of the Physics Department of the University of Rome Tor Vergata (Lat. 41°51'15''N, Long. 12°36'15''E) and (the EM) at the Astronomical Observatory of Pino Torinese (Lat. 45 ° 02 0 25 00 N, Long. 7 ° 45 0 53 00 E), where the sky conditions allowed observation of faint sources. During these tests, flashers, building lights, stars with apparent magnitude up to 4 and Jupiter have been observed [17, 18].

Figure 6 shows a night sky frame acquired in zenith position in the Apennine Mountains during ground tests. The observation of the various stars in the field of view allowed to obtain a first estimation of the PSF of the instrument of about 1.2 pixels, in agreement with the theoretical estimations.

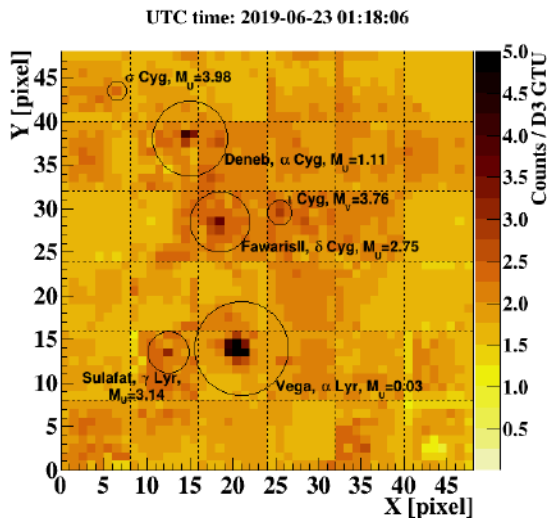


**Fig. 6** Mini-EUSO frame acquired during the field tests held in Paganico Sabino, Apennine Mountains, on June 23, 2019. The brightest visible star is Vega ( $M_u=0.03$ ), the dimmest identified star is  $\sigma$  Cyg ( $M_u=3.98$ ). Colour denotes counts/GTU ( $2.5 \mu\text{s}$ ).

## 5 Acceptance Tests and Launch

After qualification tests, the FM detector passed several acceptance tests, first in Rome, subsequently in Moscow, and finally in the Baikonur cosmodrome. Then it was then integrated in the uncrewed Soyuz MS-14 capsule and launched on 2019 August 22 (Figure 7).

After a two day flight, MS-14 was scheduled to dock with the Poisk module of the ISS on 24 August 2019, 05:30 UTC. However its Kurs automatic rendezvous system failed to lock onto the Kurs signal amplifier on ISS's Poisk docking module (due to a failure of this system, as subsequent analysis had shown) and the capsule remained at a distance of about 200 m. Docking was thus aborted and the spacecraft was repositioned on a nearby orbit, bringing it to re-approach the ISS every  $\simeq 24$  hours<sup>1</sup>. On 26 August, the three-man crew of Soyuz MS-13 relocates their spacecraft from the aft axial port of the Zvezda module and performed a manual docking at the faulty Poisk port, freeing up that port for MS-14 to dock using Kurs on 27 August 2019 at 03:08 UTC (Figure 8).



**Fig. 7** The Soyuz-MS14 rocket on its roll-out to the launch pad, 19-8-2019. This was a peculiar uncrewed flight, where a Soyuz capsule (with escape tower visible on the left part of the picture) was used to launch cargo to the ISS. This was to test a new Russian guidance system for the first time without risking a manned flight. In addition to Mini-EUSO, among the cargo was the humanoid robot Fedor.



**Fig. 8** **Left:** the first failed docking attempt on the Poisk module docking port, on 2019 August 24. **Center:** relocation of the Soyuz MS-13 capsule from the Zvezda module docking port to the Poisk module docking port. **Right:** second, successful, docking attempt on the Zvezda docking port, on 2019 August 27.

<sup>1</sup>Unmanned systems such as the cargo Progress feature backup system (called TORU) which enables cosmonauts on the station to manually control the docking of the capsules. However, since the Soyuz capsule was meant for manned spaceflight, this system was not present on the MS-14.

## 6 In-Flight Operations

The telescope was turned on for the first time on October 7, 2019 (Figure 9), after the arrival on the ISS of the cosmonaut trained to operate the instrument.



**Fig. 9** **Left:** Mini-EUSO telescope managed by the cosmonaut before to be installed on the nadir-facing UV transparent window of the Zvezda module. **Right:** Mini-EUSO mounted on the UV transparent window. The velocity vector is usually toward the bottom of the picture, in the side marked as '1'.

At the beginning of each observation session, taking place about every two weeks and of a duration of about 12 hours each, the detector is taken from storage, the lens cover is removed and the instrument is installed on the UV transparent window in the Zvezda module. Power and ground cables are connected, an USB SSD card is inserted and power is switched on. Time is kept internally with a Real Time Clock as there are no other connections with the ISS (the daily drift of the clock has been measured on ground and is periodically checked with data taken on board).

Upon startup, the system checks whether specific operational parameters intended to override the existing ones are present on the SSD card. The initialisation program also checks if software and/or firmware upgrades are present in the SSD card and in that case it uses them. This flexible approach allows for continuous improvement of operations.

At the end of each session the detector and the SSD card are stored and the log file and a subset of acquired data files are transmitted to ground through the ISS telemetry channel for analysis and verification of the correct functioning of the system. In Figure 10, left-hand side, one of the outputs of the Quick Look software showing the measurements of the UV sensors as a function of time to verify the correct handling of the day-night cycle. It is possible to see the transition between day and night every  $\simeq 45$  minutes<sup>2</sup>. Pouches with 25 SSD cards (Figure 10, right-hand side) are returned to Earth every 6-12 months and with the same temporal frequency a new pouches is sent to the ISS.

---

<sup>2</sup>The illumination period depends on the Beta angle of the ISS, the angle between the orbital plane of the station and the Sun-Earth vector. When  $\beta$  is close to  $90^\circ$  (for ISS  $\beta_{max} = 75^\circ$ ) the station is almost always illuminated by the Sun and operations are not possible. When  $\beta = 0^\circ$  the duration of the local night is the longest.

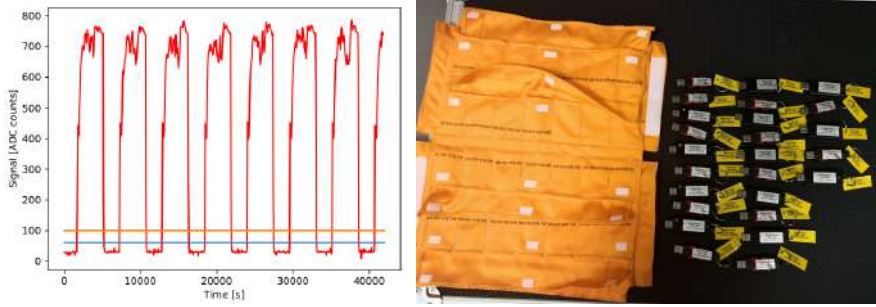


**Fig. 10** **Left:** Plot of the measurements of the UV sensor as a function of time. Mini-EUSO is operational during night-time, when the sensor measures a value below 60 ADC (Analog-to-Digital Conversion) counts. To avoid spurious fluctuations at the day-night terminator line, two thresholds are used to determine transition from day to night (60 ADC counts, blue line) and vice-versa (100 ADC counts, orange line). **Right:** Pouch containing USB pens and a sample of labelled pens.

In Figure 11 are shown the cosmonauts Oleg Novitskiy and Ivan Vagner responsible, in different periods, for the operations on the Mini-EUSO telescope.



**Fig. 11** **Left:** the cosmonaut Oleg Novitskiy with Mini-EUSO. On the bottom of the picture is visible the pouch with the data cards. **Right:** Cosmonaut Ivan Vagner with Mini-EUSO prior to its installation on the UV transparent Zvezda window (center bottom of the figure). The instrument front lens is visible between the hands of the cosmonaut.

The first session involved operation in safe mode, with only one EC unit active and the HVPS set to last dynode voltage mode, corresponding to a sensitivity of about 1% compared to the normal HVPS mode. Gradually, along the course of the following sessions, the instrument was switched on with the

full PDM active in low voltage mode and finally with the full PDM in normal voltage mode. Starting from the fifth session, the nominal acquisition configuration has been used.

Figure 12 shows the signal measured by Mini-EUSO during the first  $\sim 240$  seconds after the first switch on (in D3 mode, that is at 40.96 ms sampling rate): the telescope first flew over uninhabited areas and some cities and then detected some lightning as the measured signal was increasing for the Moon rise.

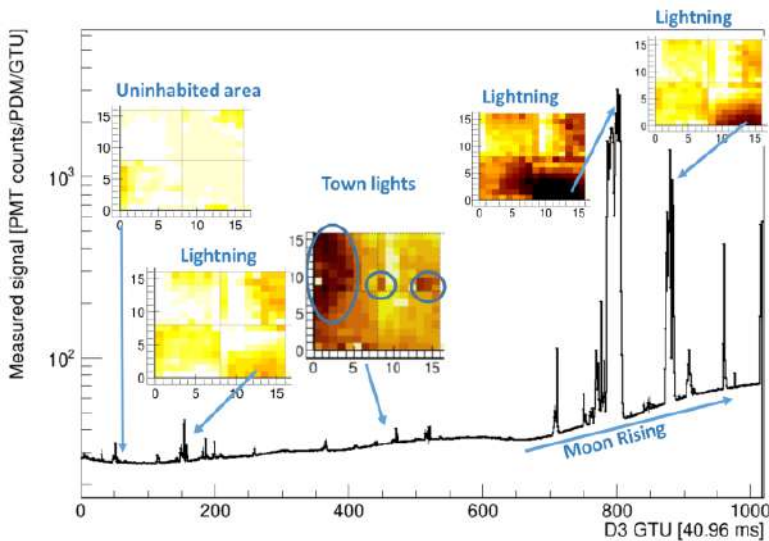


**Fig. 12** The measured signal recorded by the Mini-EUSO telescope in D3 mode (40.96 ms sampling rate) during the first  $\sim 240$  seconds of data taking of the first session, when only one EC unit was active. The signals are due to different sources: uninhabited areas, town lights and lightnings. At the end of the sequence it is possible to see the increasing of the measured counts due to the Moon rise. Each inset corresponds to the active EC unit ( $16 \times 16$  pixels).

Between October 2019 and October 2022, 70 sessions have been performed. The integrated Earth coverage up to session 44 (the last session for which the complete set of data is available on ground) is shown in Figure 13.

During the first three years of data taking, the Mini-EUSO collaboration performed also an in-flight calibration to detect the response of the instrument when exposed to a light source of measured intensity. This has been done sending LED light pulses from ground during flasher campaigns. In Figure 14 are reported two frames recorded by Mini-EUSO at  $\sim 82$  ms of temporal distance (2 frames in D3 mode) during the flasher campaign held in central Italy on May 3, 2021: some cities, such as Rome and Naples, are clearly visible and in the second frame also the flasher light is evident. Figure 15 shows the

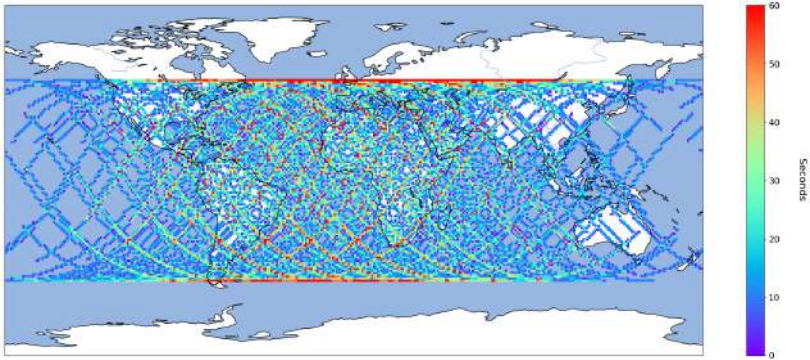


**Fig. 13** Mini-EUSO Earth coverage during the first 44 data-taking sessions. The map has been divided into  $1^\circ \times 1^\circ$  cells, the color scale represents the time spent by Mini-EUSO inside each cell.

increasing of the Mini-EUSO counts (in D3 mode) due to the flasher light detected during the same campaign.

The in-flight calibration with LED and/or laser pulses is also useful to understand the real capabilities of the instrument in detecting ultra-high energy CRs to pave the way to larger and more sophisticated space detector for the study of UHECRs from space.

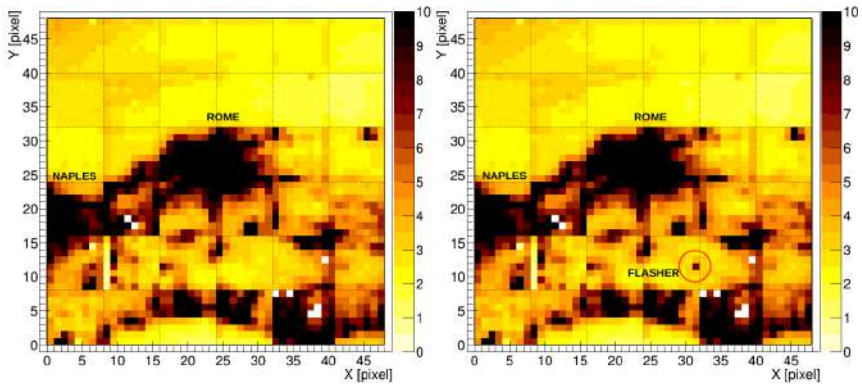


**Fig. 14** Two frames recorded by Mini-EUSO during the flasher campaign held in central Italy on May 3, 2021: some cities are clearly visible (Rome and Naples) and in the second frame, observed 2 frames in D3 mode ( $\sim 82$  ms) after the first one, , also the flasher light is marked.

## 7 Conclusions

In this work we have described the integration, qualification and acceptance tests and the launch of the Mini-EUSO telescope. The detector is currently on board the ISS performing periodic observations of the Earth from the

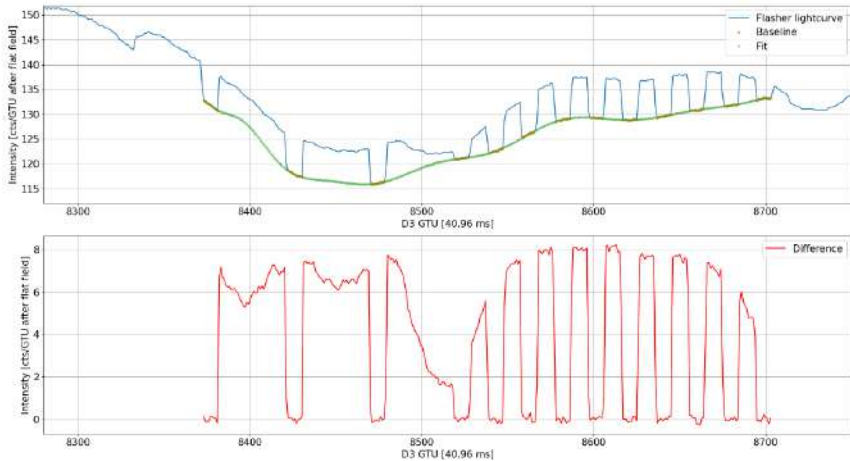


**Fig. 15** Increasing of counts due to the light detected during a flasher campaign held in central Italy on May 3, 2021. **Blue:** lightcurve of the two columns of pixels containing the UV flasher signal (see the image of the focal surface on the right). The flasher pattern is:  $6 \times [1.6\text{s ON} - 0.4\text{s OFF}] + 12 \times [0.4\text{s ON} - 0.4\text{s OFF}] \rightarrow 6 \times [39 \text{ GTU ON} - 10 \text{ GTU OFF}] + 12 \times [10 \text{ GTU ON} - 10 \text{ GTU OFF}]$ . **Green:** background estimation, fit with a 18 degrees polynomial. **Red:** flasher with background subtracted. It is possible to recognise 3(+1) long and 9(+1) short pulses.

nadir-facing UV-transparent window in the Zvezda module and it continues to behave nominally.

Data analysis is ongoing and it is very promising in many fields under investigation such as Transient Luminous Events (TLEs), in particular ELVES, meteors and nocturnal terrestrial emissions.

## 8 Acknowledgements

This work was supported by the Italian Space Agency through the agreement n. 2020-26-Hh.0, by the French space agency CNES, and by the National Science Centre in Poland grants 2017/27/B/ST9/02162 and 2020/37/B/ST9/01821.

## References

- [1] Bacholle, S., Barrillon, P., Battisti, M., Belov, A., Bertaina, M., Biscconti, F., Blaksley, C., Blin-Bondil, S., Cafagna, F., Cambiè, G., Capel, F., Casolino, M., Crisconio, M., Churilo, I., Cotto, G., de la Taille, C., Djakonow, A., Ebisuzaki, T., Fenu, F., Franceschi, A., Fuglesang, C., Gorodetzky, P., Haungs, A., Kajino, F., Kasuga, H., Khrenov, B., Klimov, P., Kochepasov, S., Kuznetsov, V., Marcelli, L., Marszał, W., Mignone, M., Mascetti, G., Miyamoto, H., Murashov, A., Napolitano, T., Olinto, A.V., Ohmori, H., Osteria, G., Panasyuk, M., Porfilio, M., Poroshin, A., Parizot, E., Picozza, P., Piotrowski, L.W., Plebaniak, Z., Prévôt, G.,

- Przybylak, M., Reali, E., Ricci, M., Sakaki, N., Shinozaki, K., Szabelski, J., Takizawa, Y., Turriziani, S., Traïche, M., Valentini, G., Wada, S., Wiencke, L., Yashin, I., Zuccaro-Marchi, A.: Mini-EUSO mission to study earth UV emissions on board the ISS. *The Astrophysical Journal Supplement Series* **253**(2), 36 (2021). <https://doi.org/10.3847/1538-4365/abd93d>
- [2] Abdellaoui, G., Abe, S., Adams, J.H., Ahriche, A., Allard, D., Allen, L., Alonso, G., Anchordoqui, L., Anzalone, A., Arai, Y., et al.: EUSO-TA - First results from a ground-based EUSO telescope. *Astroparticle Physics* **102**, 98–111 (2018). <https://doi.org/10.1016/j.astropartphys.2018.05.007>
- [3] Adams, J.H., Ahmad, S., Allard, D., Anzalone, A., Bacholle, S., Barrillon, P., Bayer, J., Bertaina, M., Bisconti, F., Blaksley, C., Blin-Bondil, S., Bobík, P., Cafagna, F., Campana, D., Capel, F., Casolino, M., Cassardo, C., Catalano, C., Cremonini, R., Dagoret-Campagne, S., Danto, P., del Peral, L., de la Taille, C., Díaz Damian, A., Dupieux, M., Ebersoldt, A., Ebisuzaki, T., Eser, J., Evrard, J., Fenu, F., Ferrarese, S., Fornaro, C., Fouka, M., Gorodetzky, P., Guarino, F., Guzman, A., Hachisu, Y., Haungs, A., Judd, E., Jung, A., Karczmarczyk, J., Kawasaki, Y., Klimov, P.A., Kuznetsov, E., Mackovjak, S., Manfrin, M., Marcelli, L., Medina-Tanco, G., Mercier, K., Merino, A., Mernik, T., Miyamoto, H., Morales de los Ríos, J.A., Moretto, C., Mot, B., Neronov, A., Ohmori, H., Olinto, A.V., Osteria, G., Panico, B., Parizot, E., Paul, T., Picozza, P., Piotrowski, L.W., Plebaniak, Z., Pliego, S., Prat, P., Prévôt, G., Prieto, H., Putis, M., Rabanal, J., Ricci, M., Rojas, J., Rodríguez Frías, M.D., Roudil, G., Sáez Cano, G., Sahnoun, Z., Sakaki, N., Sanchez, J.C., Santangelo, A., Sarazin, F., Scotti, V., Shinozaki, K., Silva, H., Soriano, J.F., Suino, G., Szabelski, J., Toscano, S., Tabone, I., Takizawa, Y., von Ballmoos, P., Wiencke, L., Wille, M., Zotov, M.: A review of the euso-balloon pathfinder for the jem-euso program. *Space Science Reviews* **218**(1), 3 (2022). <https://doi.org/10.1007/s11214-022-00870-x>
- [4] Abdellaoui, G., Abe, S., Adams, J.H., Ahriche, A., Allard, D., Allen, L., Alonso, G., Anchordoqui, L., Anzalone, A., Arai, Y., Asano, K., Attallah, R., Attoui, H., Ave Pernas, M., Bacholle, S., Bakiri, M., Baragatti, P., Barrillon, P., Bartocci, S., Bayer, J., Beldjilali, B., Belenguer, T., Belkhalifa, N., Bellotti, R., Belov, A., Belov, K., Benmessai, K., Bertaina, M., Biermann, P.L., Biktemerova, S., Bisconti, F., Blanc, N., Błęcki, J., Blin-Bondil, S., Bobik, P., Bogomilov, M., Bozzo, E., Briz, S., Bruno, A., Caballero, K.S., Cafagna, F., Campana, D., Capdevielle, J.-N., Capel, F., Caramete, A., Caramete, L., Carlson, P., Caruso, R., Casolino, M., Cassardo, C., Castellina, A., Catalano, C., Catalano, O., Cellino, A., Chikawa, M., Chiritoi, G., Christl, M.J., Connaughton, V., Conti, L., Cordero, G., Cotto, G., Crawford, H.J., Cremonini, R., Csorna, S., Cummings, A., Dagoret-Campagne, S., de Castro, A.J., De Donato, C., de la

Taille, C., De Santis, C., del Peral, L., Di Martino, M., Diaz Damian, A., Djemil, T., Dutan, I., Ebersoldt, A., Ebisuzaki, T., Engel, R., Eser, J., Fenu, F., Fernández-González, S., Ferrarese, S., Flamini, M., Fornaro, C., Fouka, M., Franceschi, A., Franchini, S., Fuglesang, C., Fujii, T., Fujimoto, J., Fukushima, M., Galeotti, P., García-Ortega, E., Garipov, G., Gascón, E., Genci, J., Giraud, G., González Alvarado, C., Gorodetzky, P., Greg, R., Guarino, F., Guzmán, A., Hachisu, Y., Haiduc, M., Harlov, B., Haungs, A., Hernández Carretero, J., Hidber Cruz, W., Ikeda, D., Inoue, N., Inoue, S., Isgrò, F., Itow, Y., Jammer, T., Jeong, S., Joven, E., Judd, E.G., Jung, A., Jochum, J., Kajino, F., Kajino, T., Kalli, S., Kaneko, I., Karadzhov, Y., Karczmarczyk, J., Katahira, K., Kawai, K., Kawasaki, Y., Kedadra, A., Khales, H., Khrenov, B.A., Kim, J.-S., Kim, S.-W., Kleifges, M., Klimov, P.A., Kolev, D., Krantz, H., Kreykenbohm, I., Krizmanic, J.F., Kudela, K., Kurihara, Y., Kusenko, A., Kuznetsov, E., La Barbera, A., Lachaud, C., Lahmar, H., Lakhdari, F., Larsson, O., Lee, J., Licandro, J., López Campano, L., López, F., Maccarone, M.C., Mackovjak, S., Mahdi, M., Maravilla, D., Marcelli, L., Marcos, J.L., Marini, A., Marszał, W., Martens, K., Martín, Y., Martinez, O., Martucci, M., Masciantonio, G., Mase, K., Mastafa, M., Matev, R., Matthews, J.N., Mebarki, N., Medina-Tanco, G., Mendoza, M.A., Menshikov, A., Merino, A., Meseguer, J., Meyer, S.S., Mimouni, J., Miyamoto, H., Mizumoto, Y., Monaco, A., Morales de los Ríos, J.A., Moretto, C., Nagataki, S., Naitamor, S., Napolitano, T., Nava, R., Neronov, A., Nomoto, K., Nonaka, T., Ogawa, T., Ogio, S., Ohmori, H., Olinto, A.V., Orleañski, P., Osteria, G., Pagliaro, A., Painter, W., Panasyuk, M.I., Panico, B., Parizot, E., Park, I.H., Pastircak, B., Patzak, T., Paul, T., Pérez-Grande, I., Peretto, F., Peter, T., Picozza, P., Pindado, S., Piotrowski, L.W., Piraino, S., Placidi, L., Plebaniak, Z., Pliego, S., Pollini, A., Polonsky, Z., Popescu, E.M., Prat, P., Prévôt, G., Prieto, H., Puehlhofer, G., Putis, M., Rabanal, J., Radu, A.A., Reyes, M., Rezazadeh, M., Ricci, M., Rodríguez Frías, M.D., Ronga, F., Roudil, G., Rusinov, I., Rybczyński, M., Sabau, M.D., Sáez Cano, G., Sagawa, H., Sahnoune, Z., Saito, A., Sakaki, N., Salazar, H., Sanchez Balanzar, J.C., Sánchez, J.L., Santangelo, A., Sanz-Andrés, A., Sanz Palomino, M., Saprykin, O., Sarazin, F., Sato, M., Schanz, T., Schieler, H., Scotti, V., Selmane, S., Semikoz, D., Serra, M., Sharakin, S., Shimizu, H.M., Shinozaki, K., Shirahama, T., Spataro, B., Stan, I., Sugiyama, T., Supanitsky, D., Suzuki, M., Szabelska, B., Szabelski, J., Tajima, N., Tajima, T., Takahashi, Y., Takami, H., Takeda, M., Takizawa, Y., Talai, M.C., Tenzer, C., Thomas, S.B., Tibolla, O., Tkachev, L., Tokuno, H., Tomida, T., Tone, N., Toscano, S., Traïche, M., Tsenov, R., Tsunesada, Y., Tsuno, K., Tubbs, J., Turriziani, S., Uchihori, Y., Vaduvescu, O., Valdés-Galicia, J.F., Vallania, P., Vankova, G., Vigorito, C., Villaseñor, L., Vlcek, B., von Ballmoos, P., Vrabel, M., Wada, S., Watanabe, J., Watts, J., Weber, M., Weigand Muñoz, R., Weindl, A., Wiencke, L., Wille, M., Wilms, J., Włodarczyk, Z., Yamamoto, T.,

- Yang, J., Yano, H., Yashin, I.V., Yonetoku, D., Yoshida, S., Young, R., Zgura, I.S., Zotov, M.Y., Zuccaro Marchi, A.: Ultra-violet imaging of the night-time earth by EUSO-Balloon towards space-based ultra-high energy cosmic ray observations. *Astroparticle Physics* **111**, 54–71 (2019). <https://doi.org/10.1016/j.astropartphys.2018.10.008>
- [5] Wiencke, L., Olinto, A., JEM-EUSO Collaboration: EUSO-SPB1 Mission and Science. *International Cosmic Ray Conference* **301**, 1097 (2017)
- [6] Klimov, P.A., Panasyuk, M.I., Khrenov, B.A., Garipov, G.K., Kalmykov, N.N., Petrov, V.L., Sharakin, S.A., Shirokov, A.V., Yashin, I.V., Zotov, M.Y., Biktemerova, S.V., Grinyuk, A.A., Grebenyuk, V.M., Lavrova, M.V., Tkachev, L.G., Tkachenko, A.V., Park, I.H., Lee, J., Jeong, S., Martinez, O., Salazar, H., Ponce, E., Saprykin, O.A., Botvinko, A.A., Senkovsky, A.N., Puchkov, A.E.: The tus detector of extreme energy cosmic rays on board the lomonosov satellite. *Space Science Reviews* **212**(3), 1687–1703 (2017). <https://doi.org/10.1007/s11214-017-0403-3>
- [7] Eser, J., Olinto, A.V., Wiencke, L.: Science and mission status of EUSO-SPB2. *PoS ICRC2021*, 404 (2021). <https://doi.org/10.22323/1.395.0404>
- [8] Klimov, P., Battisti, M., Belov, A., Bertaina, M., Bianciotto, M., Blind-Bondil, S., Casolino, M., Ebisuzaki, T., Fenu, F., Fuglesang, C., Marszał, W., Neronov, A., Parizot, E., Picozza, P., Plebaniak, Z., Prévôt, G., Przybylak, M., Sakaki, N., Sharakin, S., Shinozaki, K., Szabelski, J., Takizawa, Y., Trofimov, D., Yashin, I., Zotov, M.: Status of the k-euso orbital detector of ultra-high energy cosmic rays. *Universe* **8**(2) (2022). <https://doi.org/10.3390/universe8020088>
- [9] Olinto, A., Adams, J.H., Aloisio, R., Anchordoqui, L.A., Bergman, D.R., Bertaina, M.E., Bertone, P., Bisconti, F., Casolino, M., Christl, M.J., Cummings, A.L., De Mitri, I., Diesing, R., Eser, J., Fenu, F., Guepin, C., Hays, E.A., Judd, E.G., Krizmanic, J.F., Kuznetsov, E., Liberatore, A., Mackovjak, S., McEnery, J., Mitchell, J.W., Neronov, A., Oikonomou, F., Otte, A.N., Parizot, E., Paul, T., Perkins, J.S., Prevot, G., Reardon, P., Reno, M.H., Ricci, M., Sarazin, F., Shinozaki, K., Soriano, J.F., Stecker, F., Takizawa, Y., Ulrich, R., Unger, M., Venters, T.M., Wiencke, L., Young, R.M.: POEMMA: Probe of Extreme Multi-Messenger Astrophysics. In: , vol. 51, p. 99 (2019)
- [10] Olinto, A.V., Krizmanic, J., Adams, J.H., Aloisio, R., Anchordoqui, L.A., Anzalone, A., Bagheri, M., Barghini, D., Battisti, M., Bergman, D.R., Bertaina, M.E., Bertone, P.F., Bisconti, F., Bustamante, M., Cafagna, F., Caruso, R., Casolino, M., Černý, K., Christl, M.J., Cummings, A.L., Mitri, I.D., Diesing, R., Engel, R., Eser, J., Fang, K., Fenu, F., Filippatos, G., Gazda, E., Guepin, C., Haungs, A., Hays, E.A., Judd, E.G., Klimov,

- P., Kungel, V., Kuznetsov, E., Mackovjak, Š., Mandát, D., Marcelli, L., McEnergy, J., Medina-Tanco, G., Merenda, K.-D., Meyer, S.S., Mitchell, J.W., Miyamoto, H., Nachtman, J.M., Neronov, A., Oikonomou, F., Onel, Y., Osteria, G., Otte, A.N., Parizot, E., Paul, T., Pech, M., Perkins, J.S., Picozza, P., Piotrowski, L.W., Plebaniak, Z., Prévôt, G., Reardon, P., Reno, M.H., Ricci, M., Matamala, O.R., Sarazin, F., Schovánek, P., Scotti, V., Shinozaki, K., Soriano, J.F., Stecker, F., Takizawa, Y., Ulrich, R., Unger, M., Venters, T.M., Wiencke, L., Winn, D., Young, R.M., Zotov, M.: The POEMMA (probe of extreme multi-messenger astrophysics) observatory. *Journal of Cosmology and Astroparticle Physics* **2021**(06), 007 (2021). <https://doi.org/10.1088/1475-7516/2021/06/007>
- [11] Blin, S., Barrillon, P., de La Taille, C., Dulucq, F., Gorodetzky, P., Prevot, G.: SPACIROC3: 100 MHz photon counting ASIC for EUSO-SPB. *Nucl. Instrum. Meth.* **A912**, 363–367 (2018). <https://doi.org/10.1016/j.nima.2017.12.060>
- [12] Belov, A., Klimov, P.A., Sharakin, S.A.: The Network Architecture of the Data-processing System for the Photodetector of an Orbital Detector of Ultra-high Energy Cosmic Rays. *Instruments and Experimental Techniques* **61**, 27–33 (2018). <https://doi.org/10.1134/S0020441218010013>
- [13] Battisti, M., Barghini, D., Belov, A., Bertaina, M., Bisconti, F., Bolmgren, K., Cambiè, G., Capel, F., Casolino, M., Ebisuzaki, T., Fenu, F., Franceschi, M.A., Fuglesang, C., Golzio, A., Gorodetzki, P., Kajino, F., Klimov, P., Manfrin, M., Marcelli, L., Marszał, W., Miyamoto, H., Napolitano, T., Parizot, E., Picozza, P., Piotrowski, L.W., Plebaniak, Z., Prévôt, G., Reali, E., Ricci, M., Sakaki, N., Shinozaki, K., Szabelski, J., Takizawa, Y.: Onboard performance of the level 1 trigger of the mini-euso telescope. *Advances in Space Research* **70**(9), 2750–2766 (2022). <https://doi.org/10.1016/j.asr.2022.07.077>. *Astrophysics of Cosmic Rays*
- [14] Turriziani, S., Ekelund, J., Tsuno, K., Casolino, M., Ebisuzaki, T.: Secondary cameras onboard the mini-euso experiment: Control software and calibration. *Advances in Space Research* **64**(5), 1188–1198 (2019). <https://doi.org/10.1016/j.asr.2019.06.017>
- [15] Casolino, M., Cambiè, G., Marcelli, L., Reali, E.: Sipm development for space-borne and ground detectors: From lazio-sirad and mini-euso to lanfos. *Nuclear Instruments and Methods in Physics Research Section A: Accelerators, Spectrometers, Detectors and Associated Equipment* **986**, 164649 (2021). <https://doi.org/10.1016/j.nima.2020.164649>
- [16] Belov, A., Cambiè, G., Casolino, M., Giammanco, C., Klimov, P., Marcelli, A., Marcelli, L., Marcelli, N., Picozza, P.: Study of terrestrial and cosmic uv emissions from the international space station with the

- mini-euso telescope. *Aerotecnica Missili & Spazio* **99**(2), 93–101 (2020). <https://doi.org/10.1007/s42496-020-00047-1>
- [17] Bisconti, F., Miyamoto, H., Barghini, D., Battisti, M., Belov, A., Bertaina, M.E., Blin-Bondil, S., Cambiè, G., Capel, F., Casolino, M., Cellino, A., Conti, L., Contino, G., Cotto, G., Ebisuzaki, T., Fenu, F., Fornaro, C., Franceschi, A., Gardiol, D., Haungs, A., Klimov, P., Manfrin, M., Marcelli, L., Mignone, M., Napolitano, T., Parizot, E., Picozza, P., Piotrowski, L.W., Prévôt, G., Reali, E., Ricci, M., Shinozaki, K., Simioli, F., Suino, G., Szabelski, J.: Pre-flight qualification tests of the mini-euso telescope engineering model. *Experimental Astronomy* **53**(1), 133–158 (2022). <https://doi.org/10.1007/s10686-021-09805-w>
- [18] Barrillon, P., Battisti, M., Belov, A., Bertaina, M., Bisconti, F., Blin-Bondil, S., Bonino, R., Capel, F., Caruso, R., Casolino, M., Contino, G., Cotto, G., Dagoret-Campagne, S., Fenu, F., Fornaro, C., Forza, R., Gorodetzky, P., Guardone, N., Jung, A., Klimov, P., Manfrin, M., Marcelli, L., Mignone, M., Miyamoto, H., Mulas, R., Onorato, M., Parizot, E., Piotrowski, L., Plebaniak, Z., Prevot, G., Szabelski, J., Suino, G., Takizawa, Y., Tibaldi, P., Vigorito, C., Youssef, A.: The euso@@articleCASOLINO2021164649, title = SiPM development for space-borne and ground detectors: From Lazio-Sirad and Mini-EUSO to Lanfos, journal = Nuclear Instruments and Methods in Physics Research Section A: Accelerators, Spectrometers, Detectors and Associated Equipment, volume = 986, pages = 164649, year = 2021, issn = 0168-9002, doi = <https://doi.org/10.1016/j.nima.2020.164649>, url = <https://www.sciencedirect.com/science/article/pii/S0168900220310469>, author = M. Casolino and G. Cambie' and L. Marcelli and E. Reali, keywords = Silicon photomultipliers, Cosmic rays, Radiation, abstract = We describe some applications of SiPMs developed for space-borne detectors to be employed in astroparticle physics research. SiPMs were first installed in space in 2005 on board of the International Space Station (ISS) in the Lazio-Sirad experiment. In Lazio-Sirad the SiPMs have been used as sensors of a small calorimeter to measure radiation environment in space and assess the effectiveness of shielding for astronauts. More recently, a 64 pixel array of SiPMs was used in Mini-EUSO, an UV telescope to study UV terrestrial emissions. Mini-EUSO was launched in Summer 2019 on board the ISS and is observing the Earth from a nadir facing window in the Russian section of the station. The detector technology and readout electronics developed in these contexts can also be employed in ground-based applications, both in research and in technological transfer implementations. As an example, we also discuss the application of SiPM detectors developed for EUSO detectors in the development of Lanfos, a detector to assess the amount of Cesium in food produced in the regions affected by the 2011 Fukushima power plant accident. . project in the framework of the jem-euso program. *Experimental*

Astronomy (2022). <https://doi.org/10.1007/s10686-022-09871-8>